Thermodynamic analysis of the growth of sodium dodecyl sulfate micelles. J Phys Chem

ARTICLE *in* THE JOURNAL OF PHYSICAL CHEMISTRY · MAY 1980

Impact Factor: 2.78 · DOI: 10.1021/j100446a021

J. Phys. Chem. 1980, 84, 1044-1057

Thermodynamic Analysis of the Growth of Sodium Dodecyl Sulfate Micelles

P. J. Missel,* N. A. Mazer, G. B. Benedek, C. Y. Young,†

Department of Physics, Center for Materials Science and Engineering and Harvard-MIT Program in Health Sciences and Technology, Massachusetts Institute of Technology, Cambridge, Massachusetts 02139

and Martin C. Carey

Department of Medicine, Harvard Medical School, Division of Gastroenterology, Peter Bent Brigham Hospital and Harvard-MIT Program in Health Sciences and Technology, Boston, Massachusetts 02115 *(Received November 6, 1979)*

Publication costs assisted by the National Science Foundation

We have measured a strong increase in the size and polydispersity of SDS micelles on increasing the detergent concentration in solutions containing high salt (NaCl) concentration. The mean hydrodynamic radius $\bar{R}_h$ and the polydispersity of the micelles were measured over the following regions of temperature, detergent, and salt concentrations: 17 °C ≤ T ≤ 70 °C, 0.031 g/dL ≤ [SDS] ≤ 2 g/dL, 0.5 M ≤ [NaCl] ≤ 0.8 M, using the methods of quasielastic light scattering spectroscopy (QLS). In 0.8 M NaCl and at 20 °C, $\bar{R}_h$ increases from 60 to 218 Å as detergent concentration ranges from 0.031 to 2 g/dL. A thermodynamic theory of micelle formation and growth is presented. This theory makes use of the experimentally established result that the micelles have the shape of prolate spherocylinders. The micellar size and polydispersity is determined at each temperature and salt concentration by two chemical potentials. These are the chemical potential changes associated with transferring a detergent monomer from the solvent to either the cylindrical or spherical region of the micelle. Using only these two chemical potentials as parameters, one can predict accurately the hydrodynamic radius $\bar{R}_h$, the polydispersity, and the scattered light intensity over the entire experimental range of detergent concentration, temperature, and salt concentration. The physical origins of the chemical potentials are then analyzed from their observed magnitudes and dependence on salt concentration and temperature.

I. Introduction

In previous studies, we have employed quasielastic light scattering spectroscopy (QLS)[1,2] in conjunction with measurements of scattered light intensity and angular dissymetry[3] of scattered light intensity in order to measure the mean hydrodynamic radius ($\bar{R}_h$) and mean radius of gyration ($\bar{R}_g$), and thereby characterize the size and shape of micelles formed by sodium dodecyl sulfate (SDS) in aqueous sodium chloride solutions. A continuous transition in micellar size and shape from roughly spherical aggregates ($\bar{R}_h$ = 25 Å) to a polydisperse distribution of extended prolate spherocylindrical aggregates ($\bar{R}_h$ > 150 Å) was observed in these solutions at SDS concentrations well above the critical micellar concentration (cmc). Moreover, the distribution of micellar sizes was found to be strongly influenced by temperature and NaCl concentration. In connection with these observations, a quantitative theory of the thermodynamics of micellar growth was developed. A brief account of this theory as applied to the effects of temperature and NaCl concentration on micellar size has been given previously.[2]

In the present paper, we present a full account of this theory, explore its physical content, and analyze new experimental measurements which relate detergent concentration to the micellar size distributions. QLS measurements of $\bar{R}_h$ and deductions of micellar polydispersity (variance, V) are made on SDS micelles as a function of detergent concentration (0.031–2 g/dL) at high NaCl concentration (0.5, 0.6, and 0.8 M NaCl) for a range of temperatures (17–70 °C). Under these conditions the size distributions are found to depend strongly on SDS concentration in a manner which is accurately predicted by the present theory. In addition, it is shown that the nonexponential character of the autocorrelation function of the scattered light, a reflection of the micellar polydispersity in these solutions, is likewise accounted for by the present theory. Deductions of the weight average micellar aggregation number $\bar{n}_w$ are obtained from the QLS data as a function of SDS concentration and are compared with the results of classical light scattering studies on SDS solutions.[4-7] Finally, we utilize the theory to determine the fundamental chemical potentials responsible for the growth of SDS micelles. Such deductions provide new insights into the role of hydrophobic and electrostatic interactions in affecting the micellar size distribution.

II. Materials and Methods

A. Reagents and Solutions. The SDS used in this study was of a highly pure grade obtained from British Drug House (BDH, Poole, UK). The material was recrystallized from 95% vol/vol ethanol, and its purity (~99.5%) was verified by thin layer chromatography and by gas liquid chromatography (GLC) performed after acid hydrolysis.[8] A minor impurity was found to be ~0.5% tetradecyl sulfate, but no free alcohols were found. In our previous studies the SDS employed was obtained from Bio-Rad Laboratories (Richmond, CA) and was found, using GLC, to consist of a mixture of homologues (the C-12, C-14, and C-16 chains) with an average chain length of ~12.8 carbon atoms. This fact accounts for the difference in micellar sizes reported in this study as compared with our previous studies.[1-3] Stock solutions of our single chain length material were prepared on a weight/volume basis in the appropriate ionic strength and then diluted with the appropriate electrolyte solution to achieve the desired SDS concentrations in 0.6 and 0.8 M NaCl. The solutions were prepared for light scattering by first incubating them above the critical micellar temperature (cmt) of ~25–30 °C (25.0 °C for 0.5 M, 26.9 °C for 0.6 M, and 29.2 °C for 0.8 M

*Correspondence and reprint requests should be addressed to Paul Missel, MIT, Room 13-2018, Cambridge, MA 02139.

†Department of Physics, Brandeis University, Waltham, MA 02154.

0022-3654/80/2084-1044$01.00/0

NaCl) after which 0.5 mL of micellar solution was pipetted into an acid-washed cylindrical scattering cell (Pyrex glass, 1-mL capacity, 0.6-mm o.d.). The cell was then stoppered and centrifuged at 10 000 rpm for 5 min (Sorvall SS-1 centrifuge) to sediment dust. In order to avoid detergent precipitation, the centrifuge rotor was preheated above the cmt, and the centrifuged samples were also kept above the cmt prior to QLS measurements.

B. QLS Measurements and Data Analysis. The apparatus, temperature controls, and cumulants analysis of the autocorrelation function were identical with those employed earlier.[1-3] In what follows, we present a brief description of the method of cumulants analysis[10,11] for the characterization of the autocorrelation function.

For a polydisperse system of micelles, the homodyne autocorrelation function of the scattered light intensity, $R(\tau)$, is given by

$$R(\tau)/R(0) = [\sum_{i=1}^{\infty} G_i e^{-\Gamma_i \tau}]^2 \quad (1)$$

The decay constant Γ_i is equal to $D_i q^2$, where D_i is the diffusion coefficient of the ith micellar species, and q is the magnitude of the scattering vector. The weighting factor G_i is the fraction of intensity scattered by the ith species and is related to the concentration C_i in weight/volume, molecular weight of the aggregate, M_i, and form factor P_i as follows:

$$G_i = \frac{C_i M_i P_i}{\sum_i C_i M_i P_i} \quad (2)$$

In the cumulants analysis method, one expresses the quantity $(1/2) \ln [R(\tau)/R(0)]$ as a power series expansion in τ:[10,11]

$$\frac{1}{2} \ln \left(\frac{R(\tau)}{R(0)} \right) = \sum_{j=1}^{\infty} (-1)^j \frac{k_j}{j} \tau^j \quad (3)$$

where the coefficients, k_j, are defined as the cumulants of G_i. The first three cumulants are related to the moments of G_i:

$$k_1 = \bar{\Gamma}$$

$$k_2 = \overline{\Gamma^2} - \bar{\Gamma}^2$$

$$k_3 = \overline{\Gamma^3} - 3\overline{\Gamma^2}\,\bar{\Gamma} + 2\bar{\Gamma}^3 \quad (4)$$

where the moments $\overline{\Gamma^l}$ are defined by

$$\overline{\Gamma^l} = \sum_i G_i \Gamma^l \quad (5)$$

From the first cumulant, we deduce the mean translational diffusion coefficient $\bar{D}$ of the micelles in solution, using the following relation:

$$\bar{D} = k_1/q^2 \quad (6)$$

$\bar{D}$, in turn, is used to provide a measure of the effective mean hydrodynamic radius $\bar{R}_h$ by use of the Stokes–Einstein relation:

$$\bar{D} = \frac{k_B T}{6\pi\eta \bar{R}_h} = \sum_i G_i D_i = \frac{\sum_i C_i M_i P_i \left(\frac{k_B T}{6\pi\eta R_h(i)} \right)}{\sum_i C_i M_i P_i} \quad (7)$$

where k_B is the Boltzmann constant, T is the temperature, η is the viscosity of the solvent, and $R_h(i)$ is the hydrodynamic radius of the ith micellar species.

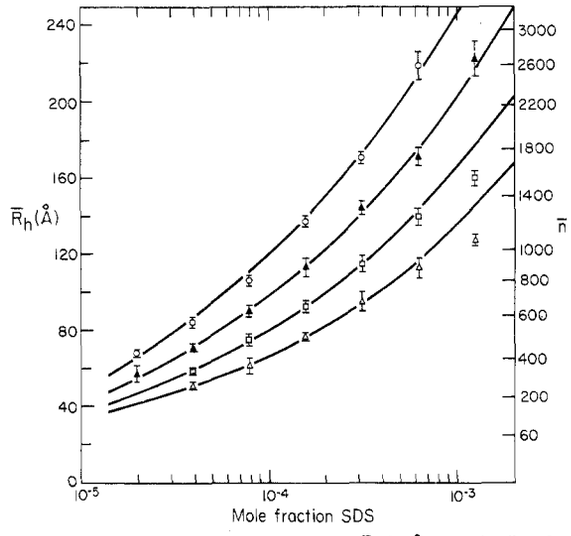

Figure 1. Concentration dependence of $\bar{R}_h$ in Å for micelles formed by SDS in 0.8 M NaCl at four temperatures: (○) 17 °C, (▲) 20 °C, (□) 25 °C, (△) 30 °C. Vertical axis on right provides a scale of mean aggregation number $\bar{n}$. Solid curves represent the fit of theory to experiment.

We characterize the width of the distribution according to the magnitude of the second cumulant through the variance as defined by Pearson:[12]

$$\text{variance } V = \frac{100 k_2^{1/2}}{k_1}\ \% = \frac{100(\overline{\Gamma^2} - \bar{\Gamma}^2)^{1/2}}{\bar{\Gamma}}\ \% \quad (8)$$

Thus, the variance provides a measure of the width of the distribution of decay rates normalized by the mean. The third cumulant (k_3) is used to provide a measure of the skewness of the distribution according to the following expression:

$$\text{skewness } S = 100 k_3 / k_2^{3/2} \quad (9)$$

A positive skewness indicates that the distribution is asymmetric, displaced toward smaller values of Γ and a negative skewness indicates displacement toward larger values of Γ.

Our cumulants analysis routine computes these quantities from the experimental autocorrelation functions by fitting $(1/2) \ln [R(\tau)/R(0)]$ to a truncated power series in τ whose order is increased until the most signigicant fit is obtained. A second-order fit is needed to deduce the first two cumulants (k_1 and k_2) from which we can determine $\bar{R}_h$ and the variance of the micellar size distribution. Higher order polynomial fits are required to obtain the skewness and kurtosis[11] of the distribution. The experimental determinations of $\bar{R}_h$ shown below represent results from several measurements averaging the two-cumulant and three-cumulant fits.

III. Results

A. Measurements of $\bar{R}_h$. QLS measurements were performed on solutions of SDS in 0.8 M NaCl as a function of SDS concentration at four temperatures (17, 20, 25, and 30 °C). The detergent concentrations studied ranged from 0.031 to 2 g/dL. However, for the purposes of our subsequent thermodynamic analysis we shall express these concentrations (denoted X) in mole fraction units (mol of SDS/mol of H_2O). Thus X varied from 1.95×10^{-5} to 1.25×10^{-3}, corresponding to a range of 3–185 times the cmc in 0.8 M NaCl ($X_{cmc} = 6.74 \times 10^{-6}$).[13] In Figure 1, the experimental values of $\bar{R}_h$ are plotted vs. SDS concentration X together with curves predicted by the theory to be presented. Under those conditions it is clearly seen that

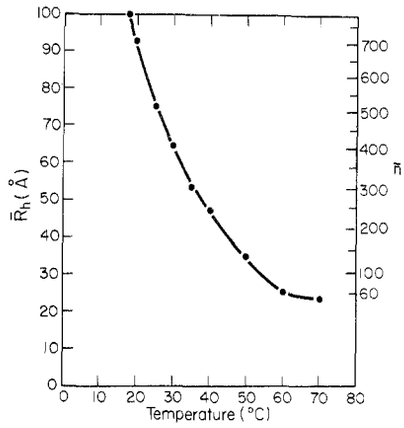

Figure 2. Temperature dependence of $\bar{R}_h$ for micelles formed in 0.6 M NaCl for the SDS concentration 2 g/dL.

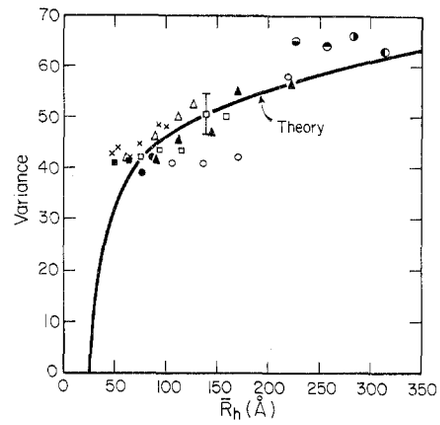

Figure 3. Variance of the micellar size distribution plotted vs $\bar{R}_h$. (X) measurements from 0.6 M NaCl with temperature ≤ 40 °C. The remaining measurements were from solutions of detergent concentration $7.8 \times 10^{-5} \leq X \leq 1.25 \times 10^{-3}$ mole fraction SDS in 0.8 M NaCl: (○) 17 °C, (▲) 20 °C, (□) 25 °C, (△) 30 °C, (●) 40 °C, (■) 50 °C. The semidarkened circles refer to measurements from solutions of detergent concentration 1.25×10^{-3} mole fraction SDS below 20 °C: (◒) 19.9 °C, (◓) 19.2 °C, (◑) 18.6 °C, (◐) 18.0 °C. Solid curve is derived from theory.

detergent concentration strongly affects the mean size of SDS micelles. At 20 °C, for example, $\bar{R}_h$ increases from ~50 to 200 Å over the range of SDS concentrations studied. Estimates of $\bar{n}$, the average aggregation number, obtained from the $\bar{R}_h$ values by assuming a prolate spherocylindrical shape are also indicated on the right-hand ordinate.[14] The largest variation of $\bar{n}$ occurs at 17 °C, where $\bar{n}$ increases from ~500 at $X = 1.95 \times 10^{-5}$ to over 2500 at $X = 6.24 \times 10^{-4}$.

In Figure 2, we present QLS measurements of $\bar{R}_h$ from solutions of SDS in 0.6 M NaCl as a function of temperature (18–70 °C) at a detergent concentration of $X = 1.25 \times 10^{-3}$ which corresponds to an SDS concentration of ~150 times the cmc ($X_{cmc} = 8.16 \times 10^{-6}$).[13] The value of $\bar{R}_h$ is seen to increase markedly as the temperature is reduced, from a value of ~23 Å at 70 °C to 100 Å at 18 °C where the solutions were appreciably supercooled below the cmt. These data are in good agreement with the results of Corti and Degiorgio, who have also used QLS to measure the size of SDS micelles.[7]

B. Dependence of V on $\bar{R}_h$. In Figure 3 we plot the variance of all solutions (see legend) vs. $\bar{R}_h$ together with the theoretical prediction for this dependence. The V values of the SDS micellar size distributions are seen to increase from ~38% to over 60% as $\bar{R}_h$ increases from 35 to over 300 Å. Such behavior is in good agreement with the theoretical dependence as will be discussed later.

IV. Thermodynamic Analysis

A. Theory of the Distribution of Micellar Sizes. As a result of hydrophobic interactions with the solvent, detergent molecules placed in solution form a distribution of micelles of various sizes. The distribution is described by the mole fraction X_n of micelles containing n detergent monomers ($n = 1, 2, 3, \ldots$). X_1 is the mole fraction of monomer in solution at equilibrium. If μ_n and μ_1 are the molar chemical potentials corresponding, respectively, to the micelle having aggregation number n and to the monomer, then, as Stigter[15] and Tanford[16] have shown, the condition of chemical equilibrium requires that

$$\mu_n = n\mu_1 \tag{10}$$

In the case of dilute solutions, μ_n and μ_1 are related to X_n and X_1 as follows:

$$\mu_n = \mu_n^0 + RT \ln X_n \tag{11a}$$

$$\mu_1 = \mu_1^0 + RT \ln X_1 \tag{11b}$$

Here, μ_n^0 and μ_1^0 are, respectively, the "standard" parts of the chemical potential for a micelle with aggregation number n and for a monomer. On inserting eq 11 into eq 10 we obtain the following equation for X_n, the distribution of micelles:

$$X_n = X_1^n \exp[-(\mu_n^0 - n\mu_1^0)/RT] \tag{12}$$

Clearly, the mole fraction X_n is determined by two physical factors. The first (X_1^n) represents the likelihood that n monomers will be *localized* in the same region of space. The second is the Boltzmann factor $\exp[-(\mu_n^0 - n\mu_1^0)/RT]$ which represents the enhancement of the micellar configuration by virtue of the chemical potential advantage $(\mu_n^0 - n\mu_1^0)$ obtained upon assembling n dissolved monomers into a single micelle. Equation 12 shows quite clearly that the micellar size distribution depends in detail upon how $(\mu_n^0 - n\mu_1^0)$ depends upon n. In fact, the precise sequence of chemical potential differences can be represented as a spectrum of energy levels, and the mole fractions X_n describe the occupancy of each of these levels.

The equilibrium properties of the dilute micellar solution can be expressed in terms of weighted averages of the properties of the individual micelles taken over the entire distribution X_n. To determine X_n theoretically, one needs to know the spectrum of energy levels $(\mu_n^0 - n\mu_1^0)$, and the equilibrium value of X_1 the mole fraction of detergent monomer in solution. The latter can be found from the constraint imposed by the conservation of matter. If X is the mole fraction of detergent monomers initially placed into solution then the conservation of matter implies the following normalization condition:

$$X = \sum_{n=1}^{\infty} nX_n \tag{13}$$

On inserting eq 12 into eq 13 we obtain a condition for X_1 as a function of X. Equations 12 and 13 along with the energy level spectrum completely determine the micellar size distribution X_n as a function of the independent variable X. The spectrum of chemical potential levels is thus basic to an understanding of the equilibrium properties of micellar solutions. Conversely, experimental data on such properties can provide information on the form of this spectrum.

B. Ladder Model for the Chemical Potential Spectrum for SDS Micelles. We now present a model for the spectrum of chemical potentials appropriate to SDS micelles. Previous experimental studies[17-20] have shown that near the cmc, SDS molecules form a minimum sized spherical

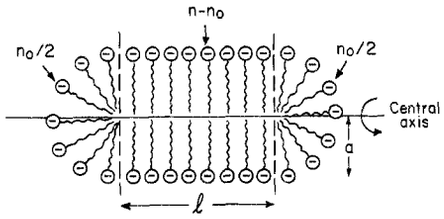

Figure 4. The structure of a prolate spherocylindrical micelle, having aggregation number n. There are $n_0/2$ molecules in each hemispherical end cap and $n - n_0$ molecules in the cylindrical region.

micelle containing n_0 ($\sim$60) monomers in pure H_2O solutions. The absence of micelles with n substantially less than n_0 implies that these micellar configurations are energetically unfavorable and hence essentially unoccupied. To obtain information on the precise form of the spectrum for $n < n_0$ requires investigations of the micellar distributions close to the cmc. Our measurements do not pertain to this region, so that as a working approximation we shall neglect the detailed distribution of levels below n_0 and approximate all such states by a single monomer state $n = 1$ and a single minimum micellar state $n = n_0$. These two states are separated by a gap $(\mu_{n_0}^0 - n_0\mu_1^0)$.

To construct a model for the levels $(\mu_n^0 - n\mu_1^0)$ for $n > n_0$, we draw upon our own experimental deductions[1-3] on the shape of SDS micelles under conditions of high SDS concentration, high ionic strength, and low temperature. These conditions represent regions of the micellar phase diagram far from the cmc. Our data and the findings of other workers[21-23] indicate that, far from the cmc, the SDS micelles take on the form of rods. More specifically they can be visualized as prolate spherocylinders as shown in Figure 4. To estimate the dependence of $(\mu_n^0 - n\mu_1^0)$ on n consistent with this geometry we first observe that the chemical potential associated with the addition of a monomer to the micelle is determined primarily by the local environment of that added monomer. The reason for this is that the principal factors which determine the additional chemical potential are the hydrophobic effect and the Debye shielded electrostatic energy. As has been suggested by Tanford,[24] one may assume to a first approximation that the chemical potential associated with a monomer in a micelle is simply a function of the area per molecule at the surface of the micelle. This area will depend upon the geometry and packing of monomers in the micelle. In the case of the prolate spherocylinder there are two distinct portions of the micelle. The first portion consists of the hemispherical end caps having n_0 monomers and a total chemical potential of $\mu_{n_0}^0$. The second portion is the cylinder. If we associate the same chemical potential μ^0 with each of the monomers in this cylindrical region, neglecting the fact that the first few monomers near the ends of the cylinder may have somewhat different values of the chemical potential, we can write the chemical potential associated with a micelle containing n monomers as

$$\mu_n^0 = \mu_{n_0}^0 + (n - n_0)\mu^0 \tag{14}$$

Each level in the spectrum of chemical potentials for $n \geq n_0$ has the form

$$\mu_n^0 - n\mu_1^0 = (\mu_{n_0}^0 - n_0\mu_1^0) + (n - n_0)(\mu^0 - \mu_1^0) \tag{15}$$

We now see that the entire spectrum of energy levels for $1 \leq n \leq \infty$ is an infinite ladder with a gap. The first state (taken as the reference energy) corresponds to the monomer state. The minimum micellar state at $n = n_0$ is spaced by a gap $(\mu_{n_0}^0 - n_0\mu_1^0)$ from the monomer state. All the subsequent states for $n > n_0$ are equally spaced with a "rung spacing" of $(\mu^0 - \mu_1^0)$. This sequence of energy levels is illustrated in Figure 5 in which we list the aggregation number n of each configuration, the associated chemical potential, and the occupancy X_n of each level. The diagram shows clearly that there are two basic parameters in this model of the energy level spectrum. The first parameter is the gap spacing Δ defined as

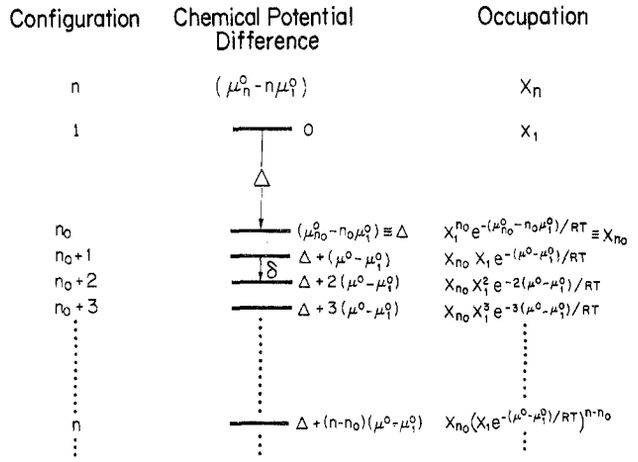

Figure 5. The diagram of chemical potential differences and the occupancies of each micellar configuration.

$$\Delta \equiv \mu_{n_0}^0 - n_0\mu_1^0 \tag{16a}$$

This quantity is the energy advantage for forming a minimum micelle out of n_0 detergent monomers in solution ($\mu_{n_0}^0$ is a larger negative number than is $n_0\mu_1^0$). The second parameter is the ladder spacing

$$\delta \equiv \mu^0 - \mu_1^0 \tag{16b}$$

This quantity represents the energy advantage associated with transferring the monomer from the solvent into the cylindrical region of the micelle (μ^0 is a larger negative number than is μ_1^0). We shall presently see that our experimental data in the regime of high detergent concentration and high salt concentration permit a determination of the following linear combination of Δ and δ:

$$\Delta - n_0\delta = \mu_{n_0}^0 - n_0\mu^0 \tag{17}$$

This quantity is the difference in chemical potential associated with n_0 monomers in the cylindrical region of the micelle as compared with n_0 monomers in the hemispherical regions of the micelle. (We expect that under conditions where rodlike micelles are formed, $n_0\delta$ will be a larger negative number than is Δ.)

C. Calculation of the Micellar Size Distribution X_n using the Model of the Infinite Ladder with a Gap. Having identified a physically reasonable model for the spectrum of chemical potential levels, we can now calculate X_1 and X_n as a function of the total detergent concentration X as outlined in section IVA.

In expressing the form of the micellar size distributions it is useful to define two characteristic mole fractions X_A and X_B whose magnitudes are related to the energy gap spacing per monomer $\Delta/(n_0 - 1)$ and the ladder spacing δ as follows:

$$X_A \equiv e^{\Delta/(n_0-1)RT} \tag{18a}$$

$$X_B \equiv e^{\delta/RT} \tag{18b}$$

It is also useful to define the parameter K as

$$K = \frac{1}{X_A}\left(\frac{X_A}{X_B}\right)^{n_0} = e^{(\Delta - n_0\delta)/RT} = e^{(\mu_{n_0}^0 - n_0\mu^0)/RT} \tag{18c}$$

This parameter is the quantity which is directly deducible from our experiments.

If we now use the sequence of energy levels given in eq 15 and represented in Figure 5, we can express X_n, the micellar size distribution, in any of the following useful forms:

$$X_n = X_A\left(\frac{X_B}{X_A}\right)^{n_0}\left(\frac{X_1}{X_B}\right)^n = \frac{1}{K}\left(\frac{X_1}{X_B}\right)^n \quad (19a)$$

$$X_n = X_A\left(\frac{X_1}{X_A}\right)^{n_0}\left(\frac{X_1}{X_B}\right)^{n-n_0} \quad (19b)$$

From eq 19a we see that the X_n distribution is a monotonically decreasing geometric sequence, provided that X_1 is smaller than X_B (a result that is necessary for the sum in eq 13 to be finite). The precise value of X_1 is determined from the total detergent concentration X by using the normalization condition eq 13 which in the present case becomes

$$X = X_1 + \sum_{n=n_0}^{\infty} nX_n \quad (20)$$

On inserting eq 19b into eq 20 we find the desired relationship between X and X_1:

$$X = X_1 + \frac{1}{K}\left(\frac{X_1}{X_B}\right)^{n_0}\left\{\frac{n_0}{(1 - X_1/X_B)} + \frac{X_1/X_B}{(1 - X_1/X_B)^2}\right\} \quad (21a)$$

The first term on the right-hand side of eq 21a is the mole fraction of detergent in the form of monomers. The second term on the right-hand side is the mole fraction of detergent monomers in the hemispherical portions of the micelle. The third term on the right-hand side is the mole fraction of monomers in the cylindrical portions of the micelles. We observe from eq 21a that X_1 never exceeds X_B, the characteristic mole fraction corresponding to the ladder spacing. The precise functional relationship between X_1 and X depends upon the relative sizes of X_A and X_B. In Appendix I we provide a detailed analysis of the form of X_1 vs. X along with a number of useful analytic approximations.

It is appropriate at this point to employ some results obtained in Appendix I, since they apply for the values of X_A, X_B, and X which occur in our experiments. For values of X much greater than the maximum monomer concentration X_B, X_1 will approach X_B. Substituting X_B for X_1 in the first term of eq 21a, we may express the quantity $K(X - X_B)$ as a function of (X_1/X_B) as follows:

$$K(X - X_B) \cong \left(\frac{X_1}{X_B}\right)^{n_0}\left\{\frac{n_0}{(1 - X_1/X_B)} + \frac{X_1/X_B}{(1 - X_1/X_B)^2}\right\} \quad (21b)$$

From this result it is seen that the quantity $K(X - X_B)$ determines the value of X_1/X_B and thereby fixes the geometric decay of the size distribution X_n. As a special case it can be shown that for $K(X - X_B) >> n_0^2$, the value of (X_1/X_B) will be approximately given by

$$\frac{X_1}{X_B} \simeq 1 - \frac{1}{[K(X - X_B)]^{1/2}} \quad (22)$$

Using this expression for (X_1/X_B) in eq 19a, we obtain the following remarkably simple result for X_n:

$$X_n \simeq \frac{1}{K}e^{-n/[K(X-X_B)]^{1/2}} \qquad n \geq n_0 \quad (23)$$

Thus the micellar size distribution is a monotonically decreasing exponential function of n ($n \geq n_0$) whose width increases in direct proportion to $[K(X - X_B)]^{1/2}$.

Of course, in general eq 21a determines X_1 as a function of X, regardless of the size of X. On using the resulting functional relation $X_1(X)$ in eq 19a, the micellar size distribution X_n is completely determined as a function of X.

Many of the relations derived here for the ionic detergent micellar system have in fact been obtained in other contexts. Israelachvilli et al.[25] have used a sequence of chemical potential differences equivalent to that appearing in Figure 5 of this paper and have derived similar expressions for the normalization condition eq 21a and the micellar size distribution eq 23. Tausk and Overbeek[26] have also adopted a similar approach for rodlike micelles formed by short-chain lecithin molecules. A review of current theoretical analyses of micelle formation has recently been given by Wennerstrom and Lindman.[27]

Mukerjee[23] has stressed the usefulness of the characterization of the polydispersity in terms of the moments of the micellar size distribution. Since we know the X_n for our ladder model we can calculate these moments directly in terms of the detergent concentration X. The number average aggregation number $\bar{n}_N$ is defined as

$$\bar{n}_N \equiv \sum_{n=n_0}^{\infty} nX_n / \sum_{n=n_0}^{\infty} X_n \quad (24a)$$

which becomes, in the limit $K(X - X_B) \gg n_0^2$, using eq 23

$$\bar{n}_N \cong n_0 + [K(X - X_B)]^{1/2} \quad (24b)$$

In a similar way the weight average aggregation number $\bar{n}_W$, defined by

$$\bar{n}_W \equiv \sum_{n=n_0}^{\infty} n^2X_n / \sum_{n=n_0}^{\infty} nX_n \quad (25)$$

can be expressed in terms of $K(X - X_B)$, in the limit $K(X - X_B) \gg n_0^2$ as

$$\bar{n}_W \cong n_0 + 2[K(X - X_B)]^{1/2} \quad (26)$$

Thus, in this limit the ratio $\bar{n}_W/\bar{n}_N$ approaches a value of 2, identical with the result obtained by Mukerjee.[28] Thus according to the present theory both $\bar{n}_N$ and $\bar{n}_W$ will approximately increase with the square root of detergent concentration.

D. Theoretical Calculations of Experimentally Observed Quantities. Having obtained expressions for X_n in terms of $K(X - X_B)$, we may use eq 1–9 to calculate the various experimentally measured quantities (i.e., $\bar{R}_h$, V, etc.) as functions of $K(X - X_B)$.

(i) Calculations of $\bar{R}_h$, V, and $R_s(\tau)/R(0)$. From eq 7 it is apparent that $\bar{R}_h$ is given by the formula[29]

$$\frac{1}{\bar{R}_h} = \frac{\sum_n n^2X_nP_n(1/R_h(n))}{\sum_n n^2X_nP_n} \qquad n \geq n_0 \quad (27)$$

Substituting the exact functional dependence of X_n on $K(X - X_B)$ into eq 27 and summing the various terms on a computer we obtain the functional dependence of $\bar{R}_h$ on $K(X - X_B)$, as plotted in Figure 6a. (The quantities $R_h(n)$ for the hydrodynamic radius and P_n for the form factor are fixed as functions of n by the geometry of the micelle as shown in Appendix II.) Using Figure 6a, K and its dependence on temperature and NaCl concentration can be deduced experimentally from $\bar{R}_h$ once X and X_B are known. (The method of deducing X_B from experimental

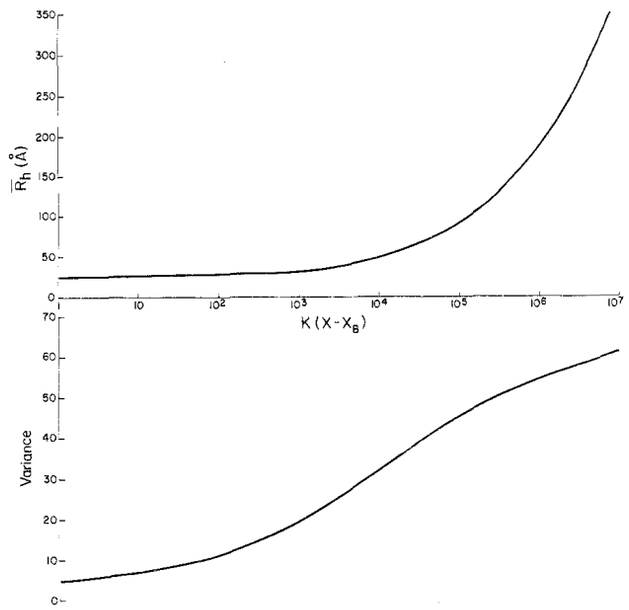

Figure 6. The theoretical dependence of (a) $\bar{R}_h$ (upper figure) and (b) variance (lower figure) vs. $K(X - X_B)$.

measurements of the cmc is described in detail in Appendix III.)

Similarly, we may use eq 8, 19, and 21b to compute V as a function of $K(X - X_B)$, as plotted in Figure 6b. Finally, given the value $K(X - X_B)$, one can calculate the exact form of the autocorrelation function $R(\tau)/R(0)$ by summing the contribution of each micellar species to the autocorrelation function as prescribed by eq 1 and 2. This calculated autocorrelation function can provide a direct comparison between the theory and experimental measurements.

(ii) Scattered Light Intensity as a Function of Detergent Concentration. In the absence of micellar interactions which introduce correlations in the relative positions of pairs of micelles, the scattered light intensity per unit solid angle I is the following weighted average:

$$I = A \sum_{n=n_0}^{\infty} n^2 X_n P_n \tag{28}$$

where A is a constant. Using this formula we can predict (to within a constant multiplicative factor A) the dependence of I on the micellar distribution X_n. Analysis of experimental data on the intensity of the light scattered from micellar solutions usually involves a Debye plot.[6,21] This is a plot of $A(X - X_1)/I$ vs. $X - X_1$. Since $X - X_1 = \sum_{n=n_0}^{\infty} nX_n$, it follows at once that

$$\frac{A(X - X_1)}{I} = \sum_{n=n_0}^{\infty} nX_n / \sum_{n=n_0}^{\infty} n^2 X_n P_n \equiv \frac{1}{\bar{n}_{w,\text{apparent}}} \tag{29}$$

If the micellar growth is not too great, then the P_n factor may be regarded as unity, we may write this equation as

$$A(X - X_1)/I \simeq 1/\bar{n}_w \tag{30}$$

This equation provides the basis by which $\bar{n}_w$ is deduced experimentally from the Debye plot. In practice, however, the interactions between micelles necessitates extrapolation to the cmc ($X - X_1 \rightarrow 0$) in order to deduce $\bar{n}_w$.

V. Comparison of Theory with Experiment

A. Deductions of K. We have calculated above the theoretical dependence of $\bar{R}_h$ and V on the quantity $K(X - X_B)$. The influence of SDS concentration on $\bar{R}_h$ is manifested through the factor $(X - X_B)$, whereas the influences of temperature and NaCl concentration result from their effects on K as given by eq 18c and ref 2. Accordingly, we may use our experimental data on the concentration dependence of $\bar{R}_h$ in 0.8 M NaCl at various temperatures (Figure 1) to test our theory as follows. Using the graph of Figure 6a, we deduce a value of the product $K(X - X_B)$ for each experimental value of $\bar{R}_h$ appearing in Figure 1. We then divide this product by the appropriate value of $(X - X_B)$, thus obtaining an estimate of K. (The values of X_B are derived from values of the cmc by the method given in Appendix III.) If our theory is correct, the values of K obtained should be the same for all values of SDS concentration at fixed temperature.

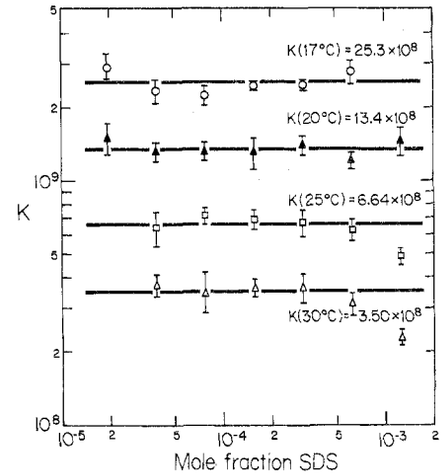

Figure 7. Plot of K vs. X for the experimental data in 0.8 M NaCl plotted in Figure 1. The horizontal lines plotted represent the average values of K for all points at a given temperature and with $X \leq 6.24 \times 10^{-4}$. These average values of K were used in calculating the theoretical curves appearing in Figure 1.

This is, in fact, demonstrated in Figure 7 where we have plotted the values of K so deduced vs. X. From this figure one can see that, in general, K is a constant at each temperature, without systematic deviation, over the entire concentration range, with the exception of the points measured at the highest concentration ($X = 1.25 \times 10^{-3}$). We suspect that the influences of intermicellar interactions would be greatest at the highest concentration, and thus may account for the depression of the two data points measured from the solutions of $X = 1.25 \times 10^{-3}$ at 25 and 30 °C. For each temperature, the values of K for all detergent concentrations below 1.25×10^{-3} mole fraction SDS were thus averaged with equal weight, and the resulting value is plotted as a solid horizontal line in Figure 7. In this manner the magnitude of K can be established for each temperature to an accuracy of ~15%.

Choosing the average value of K appropriate for each temperature, we have conversely used eq 19a, 21b, and 27b to make a comparison between the theoretical and experimental dependences of $\bar{R}_h$ on X. This comparison is presented in Figure 1. From this figure we conclude that the theory can well account for the dependence of $\bar{R}_h$ on X, using in essence one value of K for each temperature. The quantity $K(X - X_B)$ ranges from 1.37×10^4 to 1.58×10^6 for all four curves combined. Thus the agreement of theory with experiment is tested over a range of two orders of magnitude in the fundamental variable $K(X - X_B)$.

In Table Ia we have tabulated our deductions of K, X_B, and X_A and the appropriate chemical potential differences for the SDS system in 0.8 M NaCl for various temperatures. The values of K in the second column of Table Ia are those deduced by the method described above, and the corresponding values of $(\mu_{n_0}^0 - n_0\mu^0)$ appearing in the third

TABLE I: Experimental Values of the Energy Parameters for SDS

T, °C	K	$\mu_{n_0}^0 - n_0\mu^0$ kcal/mol	X_B	$\mu^0 - \mu_1^0$ kcal/mol	X_A	$(\mu_{n_0}^0 - n_0\mu_1^0)/(n_0 - 1)$
			(a) 0.8 M NaCl			
17	$(2.53 \pm 0.4) \times 10^9$	12.4 ± 0.1	7.15×10^{-6}	−6.81	8.44×10^{-6}	−6.71
20	$(1.34 \pm 0.2) \times 10^9$	12.2 ± 0.1	7.22×10^{-6}	−6.87	8.44×10^{-6}	−6.78
25	$(6.64 \pm 0.9) \times 10^8$	12.0 ± 0.1	7.27×10^{-6}	−6.98	8.39×10^{-6}	−6.90
30	$(3.50 \pm 0.6) \times 10^8$	11.8 ± 0.1	7.32×10^{-6}	−7.10	8.36×10^{-6}	−7.02
40	$(7.8 \pm 1.6) \times 10^7$	11.7 ± 0.2	7.48×10^{-6}	−7.32	8.33×10^{-6}	−7.25
50	$(2.0 \pm 0.3) \times 10^7$	10.8 ± 0.1	7.63×10^{-6}	−7.54	8.31×10^{-6}	−7.48
			(b) 0.6 M NaCl			
18	1.09×10^8	10.67	9.00×10^{-6}	−6.70	1.011×10^{-5}	−6.63
20	7.02×10^7	10.49	9.08×10^{-6}	−6.74	1.013×10^{-5}	−6.68
25	4.09×10^7	10.35	9.16×10^{-6}	−6.58	1.013×10^{-5}	−6.79
30	2.42×10^7	10.21	9.24×10^{-6}	−6.96	1.013×10^{-5}	−6.90
35	1.15×10^7	9.92	9.32×10^{-6}	−7.07	1.004×10^{-5}	−7.02
40	6.86×10^7	9.76	9.40×10^{-6}	−7.18	1.004×10^{-5}	−7.13
50	1.10×10^6	8.90	9.65×10^{-6}	−7.39	1.004×10^{-5}	−7.36

column were deduced from eq 18c. In the fourth column we report the values of X_B deduced by the method given in Appendix III, and eq 18b and 16b were used to calculate the values of $(\mu^0 - \mu_1^0)$ appearing in the fifth column of Table Ia. The appropriate values of X_A were calculated from these values of K and X_B by using the relation

$$X_A = X_B(KX_B)^{[1/(n_0-1)]} \tag{31}$$

and appear in the sixth column of Table Ia. We have used eq 18a to calculate $(\mu_{n_0}^0 - n_0\mu_1^0)/(n_0 - 1)$ and report this in the seventh column. In this manner we have succeeded in deducing the magnitudes of all the fundamental thermodynamic parameters for the SDS system in 0.8 M NaCl.

The quantity $(\mu_{n_0}^0 - n_0\mu^0)$ has a value of 12.4 kcal/mol under the conditions of 0.8 M NaCl at 17 °C where the micellar growth is most appreciable. This corresponds to a value of 12.4/60 = 0.21 kcal/mol per detergent monomer, which is small when compared with the magnitude of the gap spacing, 6.71 kcal/mol per monomer. Thus we see that a slight difference in chemical potential per monomer in the spherical and cylindrical regions of a micelle can have a large effect on micellar growth because the factor n_0 multiplies this difference in the parameter K.

Because of the success of the analysis above, we can use this method to deduce X_B, K, and X_A for data taken at one fixed detergent concentration. In Table Ib we present our deductions of these parameters and their corresponding chemical potentials for our data on $\bar{R}_h$ vs. T (shown in Figure 2) taken in 0.6 M NaCl with $X = 1.25 \times 10^{-3}$. From Table Ib, we see that over the temperature range 18–50 °C K ranges from 1.1×10^6 to 1.09×10^8, so that $K(X - X_B)$ has the range $1.38 \times 10^3 \leq K(X - X_B) \leq 1.36 \times 10^5$.

It is also worth noting that in both 0.6 and 0.8 M NaCl, for the range of temperatures studied, the ratio X_A/X_B is in all cases greater than unity. According to eq 16, 18a, and 18b this implies $|\mu_{n_0}^0 - n_0\mu_1^0|/(n_0 - 1) < |\mu^0 - \mu_1^0|$, that is, the rung spacing in the ladder of chemical potentials is larger than the gap spacing per monomer. This is the situation which is described in case II in Appendix I.

B. Dependence of V on $\bar{R}_h$. In Figure 3 we have presented the average values of the variance measured from solutions of detergent concentration $X \geq 7.8 \times 10^{-5}$, plotted vs. the corresponding $\bar{R}_h$ values. The points plotted are the averages of the variances deduced from second- and third-order cumulant fits to the autocorrelation function according to the procedure outlined in section IIB. Since for each value of $K(X - X_B)$ there is a unique value of $\bar{R}_h$, as shown in Figure 6a, one may relate a unique theoretical value of the variance with each value of $\bar{R}_h$ by referring to Figure 6b at the same value of $K(X - X_B)$. This procedure was used to generate the theoretical curve appearing in Figure 3. We conclude that the variance data indeed follow the general trend predicted by the theory over quite a substantial range in $\bar{R}_h$, from 50 Å $\leq \bar{R}_h \leq$ 300 Å.

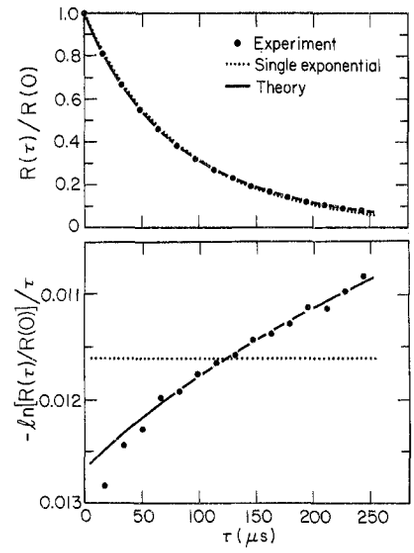

Figure 8. Plots of theoretical and experimental autocorrelation functions for the situation in which $\bar{R}_h$ = 170 Å. The experimental autocorrelation function was measured from a solution of 3.12×10^{-4} mole fraction SDS in 0.8 M NaCl at 17 °C. The theoretical autocorrelation function was generated by using a value of 2.44×10^9 for K.

C. Comparison between the Theoretical and Experimental Autocorrelation Function. While the theory is consistent with our experimental data on the variance over the range considered, there are two reasons why a more critical method of examining the width of the micellar size distribution is desired. First, there is a large experimental uncertainty in the variances calculated by the cumulants analysis process, up to ±10% in variance. Second, the variance increases in magnitude only by a factor of 1.5, from ~40 to ~60%, over the range in $\bar{R}_h$ considered here. A more vivid test of the validity of the theory consists in calculating the *direct* effect of polydispersity on the autocorrelation function itself, as this bypasses any statistical errors that are introduced in calculating the variance in the method of cumulants analysis.

In Figure 8, we illustrate a direct comparison between our computer calculation of the autocorrelation function and a sample experimental autocorrelation function. In the upper portion of the figure we plot the normalized autocorrelation function $R(\tau)/R(0)$ vs. τ for the measurement taken from a solution of 3.12×10^{-4} mole fraction

SDS in 0.8 M NaCl at 17 °C, in which $\bar{R}_h$ and V were found to be 170 Å and 43%, respectively. The solid curve represents the result of a theoretical calculation of the autocorrelation function by using a value of $K = 2.44 \times 10^9$ and the appropriate value of X_B for 17 °C. The dotted curve presented is that of a single exponential. In such a plot the autocorrelation function appears to be only slightly nonexponential. We may examine the nonexponential character of the autocorrelation function in greater detail by plotting the quantity $\ln [R(\tau)/R(0)]/\tau$ vs. τ, as is done in the lower portion of Figure 8. In such a plot, a pure exponential appears as a horizontal line, as illustrated by the dotted line, and deviations from exponential behavior become readily apparent. The data plotted in this way clearly shows a very marked deviation from a single exponential. The solid line shows the theoretical calculation of $\ln [R(\tau)/R(0)]/\tau$, using the same value of K as before. This is clearly in excellent agreement with the experimental data. We conclude that the theory can successfully describe the micellar size distribution.

D. Dependence of Scattered Intensity on X. Previous studies of the intensity of light scattered from SDS solutions have shown that the NaCl concentration affects the Debye plot.[5,7,18,19] For $C_{NaCl} \leq 0.4$ M, the Debye plots appear to be linear and have positive slope. The magnitude of this slope has been shown to be consistent with intermicellar electrostatic repulsive interactions for the case 0.1 M NaCl at 25 °C, assuming the micelles are at their minimum size independent of X.[7] Upon increasing the NaCl concentration, the slope of the Debye plot decreases due to the successive screening of the electrostatic repulsions. In fact, the slope is nearly zero for 0.4 M NaCl, and becomes negative once $C_{NaCl} \gtrsim 0.5$ M. From our previous studies[1,2] we found that SDS micelles remain close to the minimum size, independent of detergent concentration under the conditions $C_{NaCl} < 0.45$ M and $X \leq 1.25 \times 10^{-3}$. Since the Debye plot is nearly horizontal for $C_{NaCl} \sim 0.4$ M, we expect that the electrostatic repulsion is completely screened out for this and all higher NaCl concentrations. Therefore, we predict that the negative slope of the Debye plot under the conditions $C_{NaCl} \gtrsim 0.5$ M reflects the dependence of $\bar{n}_w$ on X. Excluded volume interactions may also contribute and can be accounted for with Mukerjee's approach.[23]

In fact, we find that our theory is capable of predicting the concentration dependence of the scattered light intensity without including any effects of electrostatic interactions under the conditions $C_{NaCl} \geq 0.5$ M. Once K and X_B are specified, X_n is given by eq 19a and we may use eq 29 to make a direct comparison between our theory and the experimentally obtained Debye plots. In Figure 9 we present the experimental and theoretical dependence of $1/\bar{n}_{W,apparent}$ on $(X - X_1)$. (We are assuming that $X_1 = X_{cmc}$ for $X > X_{cmc}$.) The data for 0.5 M NaCl are that of Emerson and Holtzer,[5] and the data for 0.6 M NaCl are that of Corti and Degiorgio,[7] both taken at 25 °C. These authors have in effect measured the quantity A in eq 28 and are, therefore, able to determine experimentally $1/\bar{n}_{W,apparent}$ using eq 29. We have also plotted results from our own experiments in 0.8 M NaCl at 25 °C for the concentration range $3.9 \times 10^{-5} \leq X \leq 1.25 \times 10^{-3}$. We did not measure A experimentally. Instead, we chose a value of A to fit the $1/\bar{n}_{W,apparent}$ vs. $(X - X_1)$ to the theory at one single point ($X = 6.24 \times 10^{-4}$). The solid theoretical curves for 0.6 and 0.8 M NaCl were calculated from eq 19a, 21a, and 29, using the appropriate values for K and X_B at 25 °C listed in parts a and b of Table I. The value of K for 0.5 M NaCl at 25 °C was deduced from a single QLS measurement from a solution of $X = 1.25 \times 10^{-3}$, in which $\bar{R}_h$ was found to be 42 Å. From the graph of Figure 6a, $K = 3.73 \times 10^6$, and using the method of Appendix III, we found that X_B has a value of 1.04×10^{-5}. These values of K and X_B were used to calculate the solid theoretical curve for the 0.5 M NaCl data. The dashed curves take into account the effect of the excluded volume interaction as described below.

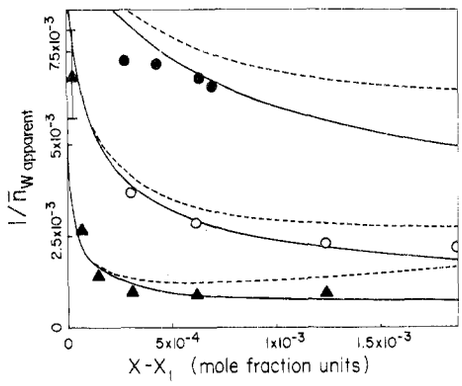

Figure 9. Deductions of $1/\bar{n}_{W,apparent}$ from classical light scattering experiments on SDS at 25 °C: (●) 0.5 M NaCl, data from Emerson and Holtzer;[5] (○) 0.6 M NaCl, data from Corti and Degiorgio;[7] (▲) 0.8 M NaCl, this study. The solid curves were calculated from eq 29a by using the values of K and X_B deduced for these conditions from QLS.

Figure 9 shows that the theory can predict the concentration dependence of the micellar molecular weight quite well: Each curve successfully reproduces the shape of the experimental Debye plots. Notice the steep upward curvature exhibited by the data in 0.8 M NaCl for small $(X - X_1)$; the curves are certainly not linear in this region. Moreover the plots for 0.5 and 0.6 M NaCl constitute a no-parameter comparison between theory and experiment, since there are no free parameters once K and X_B have been fixed by QLS and cmc experiments. Alternatively, the agreement between classical light scattering data and our data provides encouraging evidence that the results of QLS measurements are consistent with classical intensity measurements for $C_{NaCl} \geq 0.5$ M and that we have deduced the proper values for K and X_B.

The data might suggest a slight importance of the excluded volume interaction. Mukerjee[23] has demonstrated that this interaction might play an important role in determining the intensity of light scattered from solutions of high concentrations of tetradecyl hexahydroxyoxyethelene ether ($C_{14}H_{29}(OCH_2CH_2)_6OH$) in water.[30] The excluded volume interaction decreases the intensity of scattered light and should become more important with increasing detergent concentration as the micelles become larger and more numerous. The data points in Figure 9 for 0.6 and 0.8 M NaCl show that $1/\bar{n}_{W,apparent}$ is slightly larger than that predicted by our theory for the larger concentrations, reflecting a decrease in scattered intensity, and this suggests the possible importance of the excluded volume effect at higher concentrations. We therefore have used Mukerjee's[23] method of accounting for the excluded volume interactions for cylinders[31,32] to calculate the dashed curves shown in Figure 9. The data fall between the solid and dashed curves. Although the data exhibit an effect similar to that predicted by Mukerjee, more data are needed to determine the importance of this correction.

We conclude that the results of our measurements of $\bar{R}_h$ using QLS are quite consistent with previous deductions of $\bar{n}_{W,apparent}$ from classical light scattering studies. Such consistency provides additional support for our previous conclusion[1-3] that the shape of large, nonspherical SDS micelles is rodlike.

TABLE II: Thermodynamic Data on the Sphere-to-Rod Transition

	0.8 NaCl	0.6 M NaCl	0.5 M NaCl
(a) $\mu_{n_0}^0 - n_0\mu^0$ (T = 25 °C), kcal/mol	12.0 ± 0.1	10.3 ± 0.1	9.0 ± 0.2
(b) $H_{n_0} - n_0H_0$, kcal/mol	26.4 ± 0.5	25.3 ± 1.0	
(c) $S_{n_0} - n_0S_0$, kcal/(mol deg)	0.048 ± 0.002	0.050 ± 0.003	
(d) $\mu_{n_0}^{el} - n_0\mu_0^{el}$ (calcd, T = 25 °C)	−24.2	−25.6	−26.6
(e) $\bar{\mu}_{n_0} - n_0\bar{\mu}_0$ (T = 25 °C)	36.2 ± 0.1	35.9 ± 0.1	35.6 ± 0.2
(f) $\bar{H}_{n_0} - n_0\bar{H}$, kcal/mol	24.4 ± 0.5	23.3 ± 1.0	
(g) $\bar{S}_{n_0} - n_0\bar{S}$, kcal/(mol deg)	−0.040 ± 0.002	−0.042 ± 0.003	

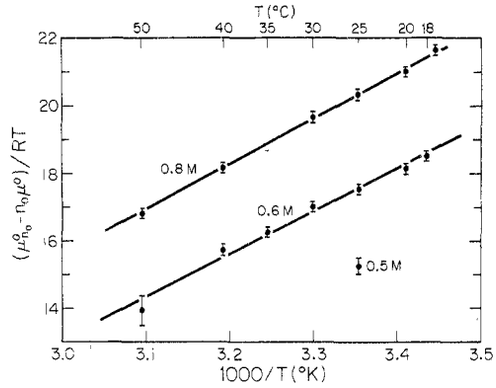

Figure 10. Experimental deductions of $(\mu_{n_0}^0 - n_0\mu^0)/RT$ vs. temperature.

VI. Discussion. Thermodynamics of the Sphere-to-Rod Transition

Having shown that our model of the sphere-to-rod transition provides an accurate description of the concentration dependence of $\bar{R}_h$ and the polydispersity of the SDS micelles, we now attempt to gain insight into the thermodynamics of this transition by analyzing our deductions of the thermodynamic parameter K.

In Figure 10, we plot the logarithm of K (equivalently $(\mu_{n_0}^0 - n_0\mu^0)/RT$) as a function of inverse temperature $(1/T(\mathrm{K}))$ for 0.6 and 0.8 M NaCl (and for the single point measured in 0.5 M NaCl). The data are seen to fall on straight lines that to within experimental error have the same slopes but different intercepts. The linearity of these plots implies that we can formally express $(\mu_{n_0}^0 - n_0\mu^0)$ in terms of enthalpic $(H_{n_0} - n_0H_0)$ and entropic $(S_{n_0} - n_0S_0)$ contributions that are temperature-*independent* quantities deduced from the slopes and intercepts of the plots (see Table II):

$$\mu_{n_0}^0 - n_0\mu^0 = (H_{n_0} - n_0H_0) - T(S_{n_0} - n_0S_0) \quad (32)$$

From Figure 10 we find that $(H_{n_0} - n_0H_0)$ is 26 ± 1 kcal mol^{-1} independent of NaCl concentration, whereas the apparent entropy change is positive in sign and depends on NaCl concentration.[33]

As a means of gaining a physical understanding of these results, we decompose $(\mu_{n_0}^0 - n_0\mu^0)$ into separate contributions from electrostatic and nonelectrostatic effects:

$$\mu_{n_0}^0 - n_0\mu^0 = (\mu_{n_0}^{el} - n_0\mu_0^{el}) + (\bar{\mu}_{n_0} - n_0\bar{\mu}_0) \quad (33)$$

The first term represents the difference in the electrostatic free energy between n_0 molecules arranged in a spherical micelle vs. the corresponding number of molecules arranged in a cylindrical configuration. This term is expected to depend on both NaCl concentration and temperature. The second term represents the difference in chemical potential associated with the nonelectrostatic effects (e.g., hydrophobic interaction, van der Waals forces, etc.) influencing the free energy of the spherical and cylindrical micellar structures. This term is expected to depend only on temperature. Physically, these terms both arise from the different surface densities of detergent molecules incorporated within the spherical and cylindrical structures.

In what follows we shall employ the Gouy–Chapman theory of the flat electric double layer in order to make a first-order estimate of the magnitude of $(\mu_{n_0}^{el} - n_0\mu_0^{el})$ and to assess its functional dependence on NaCl concentration and temperature. By subtracting these estimates from the experimental values of $(\mu_{n_0}^0 - n_0\mu^0)$ we can then deduce the magnitude of the nonelectrostatic term, $(\bar{\mu}_{n_0} - n_0\bar{\mu}_0)$. This approach is similar to Stigter's analysis of cmc data.[15]

According to the Gouy–Chapman theory, the free energy per unit area of double layer in an aqueous NaCl system, F^{el}, is given by[34]

$$F^{el} = \frac{2k_BT\sigma}{e}\mathcal{F}(S) \quad (34a)$$

where

$$\mathcal{F}(S) = \ln\left[S + (S^2+1)^{1/2}\right] + \frac{1}{S} - \frac{(S^2+1)^{1/2}}{S} \quad (34b)$$

$$S = \sigma\left[\frac{\pi}{2C_{NaCl}\epsilon(T)k_BT}\right]^{1/2} \quad (34c)$$

σ represents the surface charge per unit area, $\epsilon(T)$ is the dielectric constant of water as a function of temperature, e is the electron charge, and C_{NaCl} is the concentration of added NaCl (see Appendix IV). Because the radii of curvature of the cylindrical and spherical portions of the micelle are large compared to the Debye length (double layer thickness) in these solutions ($l_{Debye} \sim 3.5$ Å for 0.8 M NaCl), the flat plate approximation should be reasonable. In this approximation the difference in electrostatic free energy between the spherical and cylindrical regions of the micelle is due to the change in surface area per head group. Thus to assess the electrostatic free energy difference, we must first estimate the surface area per detergent head group associated with each shape. Assuming that the radius of the hydrophobic core of the micelle corresponds to the length of the extended detergent chain (~19 Å), and that the head groups have a length of ~3 Å and are fully ionized, we find that the surface charge per unit area for the minimum sphere is

$$\sigma_{sphere} = \frac{n_0e}{4\pi(22\ \text{Å})^2} \simeq \frac{e}{101\ \text{Å}^2} \quad (35)$$

Assuming that the volume of liquid hydrocarbon core in the minimum sphere is the same as that in the cylinder having n_0 monomers, it follows that the length of a cylinder L_{cyl} having a cross-sectional radius of 19 Å must satisfy

$$\pi(19\ \text{Å})^2L_{cyl} = V_{sphere} = \frac{4\pi}{3}(19\ \text{Å})^3 \quad (36)$$

which implies a value of L_{cyl} = 25.3 Å. Thus the surface

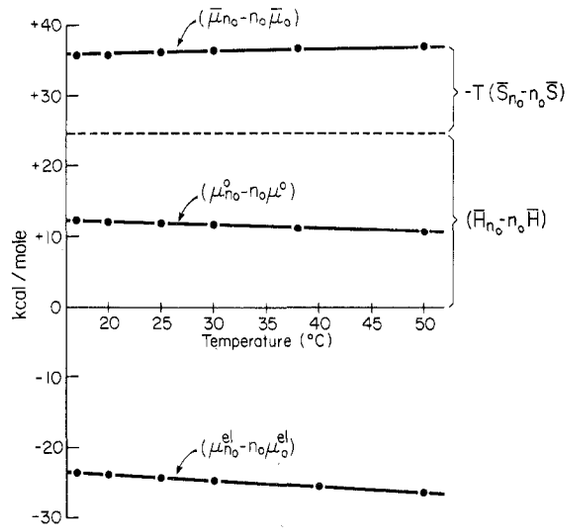

Figure 11. Temperature dependence of $\mu_{n_0}{}^0 - n_0\mu^0$ at fixed NaCl concentration (0.8 M). Also shown are the calculated values of $\mu_{n_0}{}^{el} - n_0\mu_0{}^{el}$ and the deduced values of the hydrophobic term, $\bar{\mu}_{n_0} - n_0\bar{\mu}_0$, which is broken into its enthalpic and entropic parts by the dashed line.

charge per unit area at the charge radius of 22 Å for the cylindrical geometry should be

$$\sigma_{cyl} = \frac{n_0 e}{2\pi(22\text{ Å})L_{cyl}} \simeq \frac{e}{58\text{ Å}^2} \tag{37}$$

Using these values of σ in eq 34 we may calculate the free energy difference $(\mu_{n_0}{}^{el} - n_0\mu_0{}^{el})$ as a function of C_{NaCl} and temperature.

The functional form of this result is given by

$$(\mu_{n_0}{}^{el} - n_0\mu_0{}^{el}) = 2RTn_0[\mathcal{F}(S_{sphere}) - \mathcal{F}(S_{cyl})] \tag{38}$$

where the function $\mathcal{F}$ is given by eq 34b and S_{sphere} and S_{cyl} reflect the different σ values employed in the parameter S, eq 34c. The calculated values of $(\mu_{n_0}{}^{el} - n_0\mu_0{}^{el})$ show it to be a negative quantity, whose magnitude decreases with increasing NaCl concentration (see Table II). Moreover, from eq 38 it is seen that $(\mu_{n_0}{}^{el} - n_0\mu_0{}^{el})$ is essentially proportional to temperature (the temperature dependence of S eq 34b being quite small). As a result, the electrostatic term will contribute largely to the entropic part of $(\mu_{n_0}{}^{el} - n_0\mu_0)$, as can be seen by comparing eq 32, 33, and 34. This finding is consistent with our earlier observation that the NaCl concentration primarily affected the entropic term $(S_{n_0} - n_0S_0)$. More importantly, the calculated values of $(\mu_{n_0}{}^{el} - n_0\mu_0{}^{el})$ (Table II) change with NaCl concentration by about the same amounts as does $(\mu_{n_0}{}^0 - n_0\mu^0)$. This suggests that the effect of NaCl concentration on $(\mu_n{}^0 - n_0\mu^0)$ is solely through the electrostatic term. Thus we see that despite the relative crudeness of the Gouy–Chapman picture it provides results that are both qualitatively and quantitatively consistent with the effects of temperature and NaCl concentration on K. While such consistency may be fortuitous, it is still useful to attempt a deduction of $(\bar{\mu}_{n_0} - n_0\bar{\mu}_0)$ by subtracting the calculated values of $(\mu_{n_0}{}^{el} - n_0\mu_0{}^{el})$ from the experimental values of $(\mu_{n_0}{}^0 - n_0\mu^0)$. These deductions are given in Table II where it is seen that $(\bar{\mu}_{n_0} - n_0\bar{\mu}_0)$ is ~36 kcal/mol, essentially independent of NaCl concentration. Hence, the overall tendency to micellar growth is the result of a large positive nonelectrostatic term offsetting a large negative electrostatic term. The relative importance of the two terms is illustrated in Figure 11, where $(\mu_{n_0}{}^0 - n_0\mu^0)$ is plotted as a function of temperature along with $(\mu_{n_0}{}^{el} - n_0\mu_0{}^{el})$ and $(\bar{\mu}_{n_0} - n_0\bar{\mu}_0)$ as deduced from the data in 0.8 M NaCl.

The numerical value deduced for $(\bar{\mu}_{n_0} - n_0\bar{\mu}_0)$ can be further analyzed as follows. Empirically, it has been shown[24] that the free energy of hydrophobic interaction between a hydrocarbon structure and water molecules is proportional to the hydrocarbon–water interfacial area. Neglecting any further contribution we would, therefore, expect $(\bar{\mu}_{n_0} - n_0\bar{\mu}_0)$ to be proportional to the difference in the hydrocarbon–water interfacial area between the minimum spherical micelle and the equivalent micellar cylinder. We estimate that the interfacial area associated with the minimum spherical micelle (measured at the surface of the hydrophobic core of the micelle, a radius of 19 Å from the center) will be about 1500 Å^2 larger than the interfacial area associated with the micellar cylinder:

$$A_{sphere} - A_{cyl} = 4\pi(19\text{ Å})^2 - 2\pi(19\text{ Å})L_{cyl} \cong 1500\text{ Å}^2 \tag{39}$$

Dividing $(\bar{\mu}_{n_0} - n_0\bar{\mu}_0)$ by this difference in area, we obtain a measure of the free-energy change for the hydrophobic interaction per unit area. This free-energy change is calculated from our data at 25 °C to be ~24 cal/(mol Å^2). This value is in excellent agreement with the value of 20–25 cal/(mol Å^2) deduced by Reynolds et al.[35] from solubility data as the free energy of hydrophobic interactions. Such agreement would suggest that our deduction of $(\bar{\mu}_{n_0} - n_0\bar{\mu}_0)$ is numerically reasonable and can be accounted for primarily by hydrophobic interactions.

Finally we may also estimate an enthalpy and an entropy for the hydrophobic contribution $(\bar{\mu}_{n_0} - n_0\bar{\mu}_0)$ using the weak linear dependence of $(\bar{\mu}_{n_0} - n_0\bar{\mu}_0)$ on temperature which is shown in Figure 11. These values are presented in Table II, where we have defined

$$\bar{\mu}_{n_0} - n_0\bar{\mu}_0 = (\bar{H}_{n_0} - n_0\bar{H}) - T(\bar{S}_{n_0} - n_0\bar{S}) \tag{40}$$

It should be kept in mind that the data shown in Figure 11 are sensitive to the precise magnitude and temperature dependence of the electrostatic contribution. Since this latter contribution can only be estimated approximately by using the model above, the consequent decomposition of $(\bar{\mu}_{n_0}{}^0 - n_0\bar{\mu}_0)$ into enthalpic and entropic parts must also be approximate. The enthalpic term $(\bar{H}_{n_0} - n_0\bar{H})$ is approximately 24.5 kcal/mol, accounting for roughly two-thirds of $(\bar{\mu}_{n_0} - n_0\bar{\mu}_0)$. This large enthalpy, which we have attributed to hydrophobic interactions, is at variance with the prevailing view that the unfavorable interaction between hydrocarbon and water is largely entropic in origin.[36] Nevertheless, the importance of an enthalpic contribution to the hydrophobic effect has been suggested in other studies of alkyl sulfate[37] and bile salt[38] micelles and in direct calorimetric measurements.[39] In the present case, it is worth noting that the enthalpic term $(\bar{H}_{n_0} - n_0\bar{H})$ is almost completely responsible for the temperature dependence of K, and hence the growth of the micelles as a function temperature. To demonstrate this we use eq 18c, 33, and 40 to write K as

$$K(T) = \exp\left[\frac{(\bar{H}_{n_0} - n_0\bar{H})}{RT}\right] \times \exp\left[\frac{-(\bar{S}_{n_0} - n_0\bar{S})}{R}\right] \exp\left[\frac{\mu_{n_0}{}^{el} - n_0\mu_0{}^{el}}{RT}\right] \tag{41}$$

For 0.8 M NaCl, the term $\exp[(\mu_{n_0}{}^{el} - n_0\mu_0{}^{el})/RT]$ increases by a factor of 2.20, whereas the term $\exp[(\bar{H}_{n_0} - n_0\bar{H})/RT]$ increases by a factor of 363 as the temperature decreases from 80 to 20 °C. Hence, nearly all of the temperature dependence of the mean micellar size is due to the large

enthalpy term, $(\bar{H}_{n_0} - n_0\bar{H})$, that we have attributed to hydrophobic interactions.

VII. Conclusion

We have shown that it is possible to understand the mean size and polydispersity of SDS micelles using a thermodynamic analysis based on the geometric structure of the micelle. In the present spherocylindrical model (Figure 4), first proposed by Debye and Anacker,[21] the configurations of monomer, minimum spherical micelles, and spherocylindrical micelles of different lengths can be represented by a sequence of chemical potential levels. This sequence (Figure 5) consists of a monomer state, then a gap until the minimum micellar state, followed by an infinite ladder of equally spaced rungs corresponding to increasing lengths of the spherocylinders. Basically, two parameters (chemical potential differences) are required to characterize the system at each temperature and salt concentration. These correspond to the gap spacing per monomer and the rung spacing. The occupancy of each of these levels at each temperature, detergent, and salt concentration fully determines the cmc, the micellar size distribution, and hence the experimentally observed quantities such as $\bar{R}_h$, the variance, the shape of the autocorrelation function, and the scattered intensity. By comparing the theory with the data we have deduced the fundamental chemical potentials as a function of salt and temperature. Finally, we have quantitatively analyzed these thermodynamic data in terms of the electrostatic and hydrophobic interactions affecting micellar growth. Calculations of the electrostatic terms, using the Gouy–Chapman theory, are found to be in good agreement with the observed influence of NaCl concentration on the micellar size distribution. The resulting deductions of the hydrophobic free energy are shown to be compatible with previous estimates derived from solubility experiments and suggest, in the present case, the importance of an enthalpic contribution.

Acknowledgment. G. Benedek gratefully acknowledges the fruitful intellectual atmosphere provided by Professor W. Kanzig and the Department of Physics of the Eidgenossische Technische Hochschule Zurich, where he served as Guest Professor of Physics while working out portions of the theory presented here. N. A. Mazer thanks the Connecticut Mutual Life Insurance Co. for an Insurance Medical Scientist Scholarship. This research is supported in part by the M.I.T. Center for Materials Science and Engineering, NSF Grant No. DMR 76-80895 and by NSF Grant No. CHE 77-07666 (G. B. Benedek); NIH Research Grant No. AM 18559 and Research Career Development Award AM 00195 (M. C. Carey).

Appendix I

The Normalization Condition X_1. We examine the following relationship between X_1 and X contained in the normalization condition of eq 12:

$$\frac{X}{X_A} = \frac{X_1}{X_A} + n_0\left(\frac{X_1}{X_A}\right)^{n_0}\left\{\frac{1}{\left(1 - \frac{X_1}{X_B}\right)} + \frac{\frac{1}{n_0}\frac{X_1}{X_B}}{\left(1 - \frac{X_1}{X_B}\right)^2}\right\} \tag{A-1}$$

We shall also examine the form of the micellar size distribution X_n as a function of X. The form of the dependence of X_1 on X depends on the relative size of the parameters X_A and X_B defined in eq 18a and 18b. We consider first the case $X_A < X_B$.

Case 1. $X_A < X_B$. In this case the gap spacing per particle $(\Delta/(n_0 - 1))$ is numerically larger than the ladder spacing δ; the energy advantage for forming a minimum micelle containing n_0 monomers is greater than that for assembling those n_0 monomers in the cylindrical region of a micelle. Under these conditions, we may expect that at relatively low detergent concentration ($X \lesssim X_A$) the micellar distribution will consist principally of minimum size micelles. The rodlike states ($n \gg n_0$) are substantially occupied only when X becomes sufficiently large.

Equation A-1 shows that X increases markedly with X_1 as X_1 exceeds X_A, *and* as X_1 approaches X_B. To examine analytically the relationship between X and X_1 we therefore divide the range of X_1 into two distinct regimes:

regime a $$0 < X_1 \lesssim X_A$$

regime b $$X_A \lesssim X_1 < X_B\left(1 - \frac{1}{n_0}\right)$$

We now discuss X_1 vs. X in each of these regimes.

Regime a. Here the factor $(X_1/X_A)^{n_0}$ is so small that only the X_1 term on the right-hand side of eq A-1 is important. Thus $X = X_1$. Here essentially all the added detergent appears in the form of monomers in solution. The micellar configurations are essentially unoccupied.

Regime b. Here X changes with X_1 so rapidly that it is useful to consider the values of X produced as X_1 exceeds X_A by multiples of a small scale factor ϵ, where $\epsilon \equiv (\ln n_0)/n_0$. Since $n_0 \simeq 60$, $\epsilon \cong 0.07$. The fractional changes in X_1 around X_A will be expressed as multiples of the scale factor by the relationship

$$(X_1 - X_A)/X_A = p\epsilon \tag{A-2}$$

It is convenient to consider the values of X_1 produced for integer values of p. Indeed, the full domain of regime b is spanned as p takes on the values $p = -1, 0, 1, 2, \ldots, M$. Here

$$M = \left(X_B\left(1 - \frac{1}{n_0}\right) - X_A\right) \Big/ X_A \tag{A-3}$$

and M is assumed to be large compared to unity.

In the vicinity of X_A, as X_1 changes, the consequent changes in X in eq A-1 are produced primarily by the term $(X_1/X_A)^{n_0}$. The term in curly brackets which we denote as $J(X_1)$ is approximately constant, and we shall denote its value by $J(X_A)$. Approximately $J(X_A) \simeq 1/(1 - X_A/X_B)$. Under these conditions the relationship between X_1 and X takes the form

$$X/X_A = (1 + p\epsilon) + n_0^{p+1}J(X_A) \tag{A-4}$$

Thus, for each unit increase in p, the factor (X/X_A) increases essentially by a multiple of n_0. X becomes an extremely strong function of X_1 for $X_1 \gtrsim X_A$. Indeed it is easy to show that the following analytical approximation well describes the relationship between X and X_1 in this region:

$$\frac{X - X_A}{X_A} \cong n_0J(X_A)\exp\left[n_0\left(\frac{X_1 - X_A}{X_A}\right)\right] \tag{A-5}$$

Furthermore since the second term on the right-hand side of eq A-4 represents the amount of added detergent in the form of minimum micelles, we see that as X exceeds X_A almost all of the added material appears in the form of minimum size micelles. The monomer concentration remains close to X_A, which thus corresponds to the cmc.

As X_1 increases beyond X_A and comes closer to X_B, the curly bracket term $J(X_1)$ grows from $J(X_A) \simeq 1/(1 -$

$(X_A/X_B))$ until at $X_1 = X_B(1 - 1/n_0)$ both terms in the bracket become equal in size. This signifies that equal amounts of monomer are to be found in spherical and cylindrical micellar regions. At the end of regime b

$$J(X_1) \rightarrow \{n_0 + n_0\} \qquad X_1 \rightarrow X_B\left(1 - \frac{1}{n_0}\right) \tag{A-6}$$

At this point the corresponding value of X is given by

$$\frac{X - X_B}{X_A} \cong (2/e){n_0}^2\left(\frac{X_B}{X_A}\right)^{n_0} \tag{A-7}$$

In view of the fact that ${n_0}^2 \geq 10^3$ and that $(X_B/X_A)^{n_0}$ is presumed large compared to unity, it becomes virtually impossible to experimentally attain values of X which reach the limit defined in eq A-7. Thus we must conclude that if $X_A < X_B$ to all intents and purposes no substantial micellar growth takes place as X increases above the cmc (X_A).

Case 2. $X_B < X_A$. In this case the gap spacing per particle is smaller than the ladder spacing. The energy advantage of forming n_0 monomers in the cylindrical region of the micelle is greater than that for forming n_0 monomers into a minimum spherical micelle. In our experiments the quantity KX_B ranges from 10 to 10^4. Since $[(X_A - X_B)/X_B] \simeq (\ln KX_B)/(n_0 - 1)$ we find that X_A exceeds X_B by an amount between ~4 and ~15% in the present experiments. Thus, case 2 applies to our data. Since $X_A > X_B$ and since X_1 ranges from 0 to X_B it is convenient to rewrite eq A-1 as follows:

$$KX = KX_1 + n_0\left(\frac{X_1}{X_B}\right)^{n_0}\left\{\frac{1}{\left(1 - \frac{X_1}{X_B}\right)} + \frac{\frac{1}{n_0}\frac{X_1}{X_B}}{\left(1 - \frac{X_1}{X_B}\right)^2}\right\} \tag{A-8}$$

where we have used eq 18c: $(1/K) = X_A(X_B/X_A)^{n_0}$. Now we may define the variable Z in terms of X_1 as

$$Z \equiv n_0\frac{X_B - X_1}{X_B} \tag{A-9}$$

Since n_0 is 60, we can write the normalization relation in terms of Z with good accuracy as

$$\frac{K(X - X_B)}{{n_0}^2} \cong -\frac{KX_B}{{n_0}^2}\left(\frac{Z}{n_0}\right) + e^{-Z}\left\{\frac{1}{Z} + \frac{1 - Z/n_0}{Z^2}\right\} \tag{A-10}$$

The corresponding full domains of X, X_1, and Z are $0 < X < \infty$, $0 \leq X_1 < X_B$, and $n_0 > Z > 0$. It is convenient to consider the X_1 vs. X relationship in three regimes: (a) $0 < X < X_B$, (b) $X \simeq X_B$, (c) $X \gg X_B$.

Regime a. $0 < X < X_B$. In the vicinity of $X = 0$, $Z = n_0$ and we may neglect both the second and third terms on the right-hand side of eq A-10. In this region eq A-10 shows that

$$\frac{X_B - X}{X_B} \cong \frac{Z}{n_0} = \frac{X_B - X_1}{X_B} \tag{A-11}$$

Thus

$$X = X_1 \qquad X \ll X_B \tag{A-12}$$

Thus in this regime all the added detergent appears as monomers.

Regime b. $X \simeq X_B$. We now consider the relationship between X_1 and X as $X \rightarrow X_B$. As $X \rightarrow X_B$ the second and third terms on the right-hand side of eq A-10 grow until at $X = X_B$ they equal the first term. At this value of X_B the relationship between X_1 and X begins to deviate from a strict equality. All the added detergent does not appear in monomer form but instead begins to appear in the form of micelles. In fact, the critical micellar concentration is in the vicinity of $X = X_B$. We now investigate the value of X_1 and the relative distribution of detergent between spherical and cylindrical regions when $X = X_B$, i.e., near the cmc. Although X_1 will be close to X_B, the precise deviation will determine sensitively whether the micelles that form initially are either spherical or rodlike. We can clearly see the value of monomer concentration $X_1 = X_1^*$, and the geometrical forms of the micelles which are produced when $X = X_B$ by examining eq A-10, which in this case becomes

$$\left(\frac{KX_B}{{n_0}^3}\right)Z^* = e^{-Z^*}\left\{\frac{1}{Z^*} + \frac{1 - \frac{Z^*}{n_0}}{Z^{*2}}\right\} \tag{A-13}$$

The solution for $Z^* \equiv n_0(X_B - X_1^*)/X_B$ depends in detail on the numerical magnitude of ${n_0}^3/KX_B$. We can distinguish three distinct subcases as follows:

Subcase i. $(KX_B/{n_0}^3) \ll 2/e$. Here, $n_0 \geq Z^* \geq 1$ and the first term in curly brackets in eq A-13 which corresponds to the material in spherical micelles is much greater than the second and thus the micelles which appear as $X \rightarrow X_B$ are primarily the minimum spherical micelles. In our experiments $1 \times 10^{-6} < KX_B/{n_0}^3 < 1 \times 10^{-3}$. Thus subcase i applies to our studies. Under these conditions the solution for Z^* can be written approximately as

$$Z^* + 2 \ln Z^* \simeq \ln ({n_0}^3/KX_B) \tag{A-14}$$

and Z^* ranges between 4 and 9 in our experiments.

Subcase ii. $(KX_B)/{n_0}^3 = 2/e$. In this case $Z^* \simeq 1$. Under these conditions both the first and second terms on the right-hand side of eq A-13 are about equal in size and the micelles formed near the cmc contain molecules distributed in roughly equal proportions between spherical and cylindrical forms, and thus the average aggregation number is $\sim 2n_0$.

Subcase iii. $KX_B/{n_0}^3 \gg 2/e$. Under these conditions $Z^* \ll 1$, and the second term on the right-hand side of eq A-13 is much larger than the first. Thus as $X \rightarrow X_B$ and the micelles first appear, they have at once the form of a broad distribution of elongated cylindrical micelles.

Regime c. $X \gg X_B$. In this domain $X_1^* < X_1 < X_B$. As $X_1 \rightarrow X_B$, $Z \rightarrow 0$ and we may neglect the first term on the right-hand side of eq A-10. Thus Z depends entirely on the quantity $K(X - X_B)/{n_0}^2$. We may again distinguish three subcases, $K(X - X_B)/{n_0}^2$ less than $2/e$, equals $2/e$, or exceeds $2/e$. In the first subcase Z exceeds unity and the distribution consists primarily of spherical micelles. In the second subcase $Z = 1$ and approximately equal amounts of material are to be found in the spherical and cylindrical configurations. Finally, in the third subcase, which is relevant to our experiments, $Z < 1$ and in this regime an appreciable micellar growth can occur. Specifically in this case we may show easily the following simple relation between Z and X:

$$Z = n_0/[K(X - X_B)]^{1/2} \tag{A-15}$$

Thus

$$\left(\frac{X_1}{X_B}\right) \cong 1 - \frac{1}{[K(X - X_B)]^{1/2}} \tag{A-16}$$

for $K(X - X_B) \gg (2/e)n_0^2$. It can further be shown that the micellar size distribution is expressed as

$$X_n = \frac{1}{K}\left(\frac{X_1}{X_B}\right)^n = \frac{1}{K}e^{-n/[K(X - X_B)]^{1/2}} \quad \text{(A-17)}$$

Thus the micellar size distribution in this limit is an exponentially decreasing function of n, whose number average mean is given by

$$\bar{n}_N = n_0 + [K(X - X_B)]^{1/2} \quad \text{(A-18)}$$

Appendix II

A. Form Factor P_n. We have used the following two approximations for the exact expression of the form factor for rodlike particles:[40]

$$P(X) \simeq [1 + X^2/9 + 7X^4/2025]^{-1} \quad \text{for } 0 < X < 2 \quad \text{(A-19a)}$$

$$P(X) \simeq \frac{\pi}{2\left(X + \frac{1}{\pi}\right)} \quad \text{for } 2 < X < \infty \quad \text{(A-19b)}$$

where

$$X = \frac{2\pi l}{\lambda'} \sin(\theta/2) \quad \text{(A-19c)}$$

Here l is the length of the rod, λ' is the wavelength of the light divided by the index of refraction, and θ is the scattering angle. For our experiments, $\lambda' \sim (4880\ \text{Å}/1.333)$ and $\theta = 90°$. All that remains to determine P_n is to specify the functional dependence of l on aggregation number n.

In Figure 4 we show our geometrical model for the SDS micelle with n molecules, a prolate spherocylinder with $n_0/2$ molecules in each hemispherical cap of radius a, and $n - n_0$ molecules in the cylinder region of length l and radius a. We may solve for the length l in terms of n, n_0, and the radius a as follows. We assume that the density of liquid hydrocarbon is the same in the cylindrical portion as it is in the hemispherical portions of the micelle. Upon equating the number of monomers per unit volume in both portions, we find that

$$\frac{n_0}{\frac{4\pi}{3}a^3} = \frac{n - n_0}{\pi a^2 l} \quad \text{(A-20)}$$

Solving for l, we find an expression in terms of n:

$$l(n) = \frac{4a}{3n_0}(n - n_0) \quad \text{(A-21)}$$

The hemispherical end caps contribute very little to the form factor for the large micelles. If we neglect the effects of the end caps, eq A-19 become

$$P_n = [1 + A(n - n_0)^2 + B(n - n_0)^4]^{-1} \quad n_0 < n < 3000 \quad \text{(A-22a)}$$

$$= [2/\pi^2 + C(n - n_0)]^{-1} \quad n \geq 3000 \quad \text{(A-22b)}$$

where we have used the fact that $a = 25$ Å and $n_0 = 60$ for SDS. The formulas used in this study for P_n are given by eq A-22a,b with the values for A, B, and C given as follows:

$$A = 5.028 \times 10^{-8} \quad \text{(A-23a)}$$

$$B = 7.079 \times 10^{-16} \quad \text{(A-23b)}$$

$$C = 4.283 \times 10^{-4} \quad \text{(A-23c)}$$

B. Equation for D_n. We may relate the mean diffusion coefficient D_n to the hydrodynamic radius $R_h(n)$ of a micelle of aggregation number n by the Stokes–Einstein relation:

$$D_n = k_B T/6\pi\eta R_h(n) \quad \text{(A-24)}$$

where k_B is the Boltzmann constant, T is the temperature, and η is the solvent viscosity. In this study, for a given value of n, we have used the formula for the hydrodynamic radius of a prolate ellipsoid whose volume is equal to that of the prolate spherocylinder with that same value of n. We chose this method since there exists an exact result for R_h only for the ellipsoids of revolution.

The hydrodynamic radius for a prolate ellipsoid of semiminor axis a and semimajor axis b is given by[41]

$$R_h(a,b) = \frac{b(1 - a^2/b^2)^{1/2}}{\ln\left[\frac{1 + (1 - a^2/b^2)^{1/2}}{a/b}\right]} \quad \text{(A-25)}$$

We have chosen the semiminor axis a to be 25 Å. All that remains is to specify the dependence of b on n. Again using a geometrical calculation, we may relate the semimajor axis b of the ellipsoid with equivalent volume and radius to that of the cylinder of length l by equating their volumes:

$$\frac{4\pi}{3}a^2 b = \pi a^2 l + \frac{4\pi}{3}a^3 \quad \text{(A-26)}$$

This implies that b has the following dependence on n:

$$b(n) = \frac{3}{4}\left(l(n) + \frac{4a}{3}\right) = a\left(\frac{n}{n_0} - 1\right) + a \quad \text{(A-27a)}$$

$$= \frac{an}{n_0} \quad \text{(A-27b)}$$

where $a = 25$ Å for SDS. Thus, using eq A-24, A-25, and A-27b one may find D_n.

Appendix III

Method of Deduction of X_B. In this appendix we describe a method of deducing X_B, once K is specified, from experimental deductions of the cmc by classical light scattering intensity measurements. In the experimental deduction of the cmc by light scattering, the intensity measurements of the light scattered from solutions of increasing detergent concentration are recorded and plotted vs. detergent concentration X. The scattered intensity increases abruptly at the point where micelles first form. Thus the cmc is determined as the point of intersection of two lines extrapolating the measured intensity of the solution from below and from above the region in which the change of slope in the curve of intensity vs. X is observed.[42] Let us define this intersection point as the "break point".

We may use our theory to generate such a curve of intensity vs. X once the values of K and X_B are specified. We may calculate the theoretical value of the intensity as a function of X_1 to within an arbitrary multiplicative constant using the following equation:

$$I = A(X_1 + \sum_{n=n_0}^{\infty} n^2 X_n) \quad \text{(A-28)}$$

where we have used eq 28 including the effect of the monomers and neglecting the effect of the form factor, setting $P_n = 1$. We should be able to neglect the form factor since we are considering a small range in X over which the micellar size should not approach the wavelength of light. X_n is given as a function of X_1 and the parameters K and X_B by eq 19a. Thus we known I as a function of X_1, K,

and X_B. Finally, we may use eq 21a to relate X_1 to X, thus deducing I as a function of X, K, and X_B.

In this manner we can simulate the experimental dependence of I vs. X for different values of K and X_B. [K is known at fixed temperature and salt concentrations from our data taken at large X. Also the experimental values of the cmc are known from the light scattering data of previous workers at 25 °C.[5] We have assumed that the experimental value of the cmc is a weak function of the temperature.] The effect of X_B on the function $I(X,K,X_B)$ is to translate the "break point" in the theoretical intensity curve to the right or left. Thus one may deduce X_B once the values of K and the experimental cmc are known by choosing the value of X_B such that the theoretical break point of the curve of $I(X,K,X_B)$ vs. X occurs at the value X = cmc.

Appendix IV

Free Energy of the Flat Electric Double Layer. According to Verwey and Overbeek,[34] the electric potential ψ_0 at the surface of an infinite flat plane with surface charge σ, in the presence of added NaCl will be given by

$$\psi_0 = \frac{2k_BT}{e} \sinh^{-1}\left(\sigma\left[\frac{\pi}{2C_{NaCl}\epsilon(T)k_BT}\right]^{1/2}\right) \qquad \text{(A-29)}$$

where $\epsilon(T)$ is the dielectric constant of the solvent and C_{NaCl} is the electrolyte concentration in ions/cm^3. The electrical free energy per unit area needed to assemble the surface charge and the associated diffuse layers is given by[15,34]

$$F_{el} = \int_0^\sigma \psi_0(\sigma')\, d\sigma' \qquad \text{(A-30)}$$

Upon integration of eq A-30 using the form given in eq A-29 we obtain the result given in eq 34. The temperature $\epsilon(T)$ for water was taken to be[43]

$$\epsilon(T) = 305.6e^{-T(K)/219} \qquad \text{(A-31)}$$

References and Notes

(1) N. A. Mazer, G. B. Benedek, and M. C. Carey, *J. Phys. Chem.*, **80**, 1075 (1976).
(2) N. A. Mazer, M. C. Carey, and G. B. Benedek in "Micellization, Solubilization, and Microemulsions", Vol. 1, K. L. Mittal, Ed., Plenum Press, New York, 1977, p 359.
(3) C. Y. Young, P. J. Missel, N. A. Mazer, G. B. Benedek, and M. C. Carey, *J. Phys. Chem.*, **82**, 1375 (1978).
(4) R. J. Williams, J. N. Phillips, and K. J. Mysels, *Trans. Faraday Soc.*, **51**, 728 (1955).
(5) M. F. Emerson and A. Holtzer, *J. Phys. Chem.*, **71**, 1898 (1967). Also M. F. Emerson, Ph.D. Thesis, Washington University, 1966.
(6) P. Debye, *N.Y. Acad. Sci. Ann.*, **51**, 575 (1949).
(7) M. Corti and V. Degiorgio, *Ann. Phys.*, **3**, 303 (1978).
(8) Hydrolysis was performed by dissolving the detergent in 1 N HCl, heating this solution to 100 °C for 1 h, and extracting with hexanes.
(9) A. Smith, *J. Colloid Interface Sci.*, **66**, 575 (1978).
(10) D. E. Koppel, *J. Chem. Phys.*, **57**, 4814 (1972).
(11) N. A. Mazer, S.B. Thesis, MIT, 1973.
(12) M. G. Kendall and A. Stuart, "The Advanced Theory of Statistics", Vol. 1, Hafner Publishing Co., New York, 1969, p 47.
(13) This value is extrapolated by using the equation given in ref 5 based on cmc data taken over the range 0 M $\leq C_{NaCl} \leq$ 0.5 M.
(14) The values of $\bar{n}$ are determined from the equation $\bar{n} = n_0(a_1(\bar{R}_h))/25$, where $a_1(\bar{R}_h)$ is the semimajor axis (in Å) of a prolate ellipsoid having hydrodynamic radius $\bar{R}_h$ and a semiminor axis of 25 Å, and n_0 is the aggregation number of the minimum spherical micelle (taken to be 60). See ref 2. These $\bar{n}$ values correspond roughly to a "weight" average (see N A. Mazer, Ph.D. Thesis, M.I.T., 1978).
(15) D. Stigter, *J. Colloid Interface Sci.*, **47**, 473 (1974).
(16) C. Tanford, *Science*, **200**, 1012 (1978).
(17) H. Coll, *J. Phys. Chem.*, **74**, 520 (1970).
(18) F. Huisman, *Proc. Kon. Ned. Akad. Wet., Ser. B*, **67**, 367, 376, 388, 407 (1964).
(19) K. J. Mysels and L. H. Princen, *J. Phys. Chem.*, **63**, 1696 (1959).
(20) N. J. Turro and A. Yekta, *J. Am. Chem. Soc.*, **100**, 5951 (1978).
(21) P. Debye and E. W. Anacker, *J. Phys. Colloid Chem.*, **55**, 644 (1951).
(22) D. Stigter, *J. Phys. Chem.*, **70**, 1323 (1966).
(23) P. Mukerjee, *J. Phys. Chem.*, **76**, 565 (1972).
(24) C. Tanford, *J. Phys. Chem.*, **78**, 2469 (1974).
(25) J. N. Israelachvilli, D. J. Mitchell, and B. W. Ninham, *J. Chem. Soc., Faraday Trans. 2*, **72**, 1525 (1976).
(26) R. Tausk and J. Th. G. Overbeek, *Colloid Interface Sci.*, **2**, 379 (1976).
(27) H. Wennerstrom and B. Lindman, *Phys. Rep.*, **52**, No 1 (1979).
(28) This size distribution index differs, however, from that given by Tanford (C. Tanford, *J. Phys. Chem.*, **78**, 2469 (1974)). The difference arises because Tanford uses oblate and prolate ellipsoids for the micellar geometry, and thus the dependence of μ_n^0 on n is weaker than linear. Hence his size distribution indicies are closer to 1, even for the prolate ellipsoid. See also J. E. Liebner and J. Jacobus, *J. Phys. Chem.*, **81**, 130 (1977).
(29) Here we change from the index i to n, allowing n to vary from n_0 to infinity, and we have substituted the quantity n^2X_n for C_iM_i.
(30) R. R. Balmbra, J. S. Clunie, J. M. Dorkill, and J. F. Goodman, *Trans. Faraday Soc.*, **60**, 979 (1967).
(31) The correction for the excluded volume interaction has the form $1/\bar{n}_W$ apparent $= (1 + 8\bar{v}cf)/\bar{n}_W$, where $\bar{v}$ is the partial specific volume of the micelles, c is the concentration of material in micellar form (expressed in g/mL), and f is a shape factor, departing from unity as the micelles become more rodlike. For cylinders, $f = (\pi r^2 + (\pi + 3)rl + l^2)/8rl$, where r is the radius and l is the length of the cylinder (see ref 23). After expressing l as a function of n using the first term in eq A-21, we may take the following average over X_n to obtain the correction for the excluded volume effect including polydispersity:

$$8\bar{v}cf = (0.86)(16.021)\sum_{n=n_0}^{\infty} nX_n(4n/3n_0 + (\pi + 3) + 3\pi n_0/4n)$$

where we have taken $\bar{v}$ to be 0.86 mL/g as reported in ref 32 for SDS, and where the factor 16.021 arises from converting from mole fraction units to mL/g.
(32) M. Kodama and M. Miura, *Bull. Chem. Soc. Jpn.*, **45**, 2265 (1972).
(33) That the enthalpy change $H_{n_0} - n_0H_0$ is roughly independent of NaCl concentration has been shown in our earlier work (ref 2) over a wide range of concentration (0.15–0.6 M NaCl). The value obtained in that study, 34 kcal/mol, is larger than the present deduction due to the presence of higher chain length alkyl sufates (C_{14} and C_{16}) in the earlier samples.
(34) E. J. Verwey and J. Th.G. Overbeek, "Theory of the Stability of Lyophobic Colloids", Elsenier, Amsterdam, 1968.
(35) J. A. Reynolds, D. B. Gilbert, and C. Tanford, *Proc. Natl. Acad. Sci. U.S.A.*, **71**, 2925 (1974).
(36) C. Tanford, "The Hydrophobic Effect", Wiley, New York, 1973, Chapter 4.
(37) E. A. G. Aniansson, S. N. Wall, M. Almgren, H. Hoffman, I. Kielman, W. Ulbicht, R. Zana, J. Lang, and C. Tondre, *J. Phys. Chem.*, **80**, 905 (1976).
(38) N. A. Mazer, M. C. Carey, R. F. Kwasnick, and G. B. Benedek, *Biochemistry*, **18**, 3064 (1979).
(39) S. J. Gill, N. F. Nichols, and I. Waadso, *J. Chem. Thermodyn.*, **7**, 175 (1975).
(40) B. H. Zimm, *J. Chem. Phys.*, **16**, 1099 (1948).
(41) B. Chu, "Laser Light Scattering", Academic Press, New York, 1974, p 212.
(42) E. Ruckenstein and R. Nagarajan, *J. Colloid Interface Sci.*, **57**, 388 (1976).
(43) R. W. Gurney, "Ionic Processes in Solution", McGraw-Hill, New York, 1931, p 16.